JOURNAL OF MATERIALS SCIENCE 37 (2002) 4137–4144

Characterisation of $Ce_{0.8}Gd_{0.2}O_{1.9}$/3Y-TZP composite electrolytes—Effects of 3Y-TZP particle treatment

R. J. BALL, R. STEVENS
Department of Engineering and Applied Science, University of Bath, Bath, BA2 7AY, UK
E-mail: R.J.Ball@Bath.ac.uk

Solid oxide fuel cell (SOFC) electrolytes are currently manufactured from yttria stabilised zirconia. A limitation of this material is the high operating temperatures needed for efficient operation, approximately 1000°C, as this can lead to sealing problems and require expensive nickel/chromium alloy auxiliary components. Alternative electrolytes, which allow operation at reduced temperatures, such as gadolinium doped cerium oxide have been suggested. However these ceramic materials often exhibit inferior mechanical properties. In this paper the manufacture and characterisation of composite electrolytes consisting of 3% yttria stabilised zirconia particles in a 20% gadolinia doped ceria matrix is described. Results suggest improvements in strength can be achieved by the composite approach.

1. Introduction

Solid oxide fuel cells (SOFC's) are attracting substantial interest due to their versatility and ability to operate at high efficiencies. Presently, efficiencies of around 60% for single systems and up to 85% for combined heat and power systems are achievable [1]. SOFC's react hydrogen, methane or other carbon based fuels in an electrochemical process producing electricity. Water vapour is generally expelled making it an appropriate alternative to more highly polluting conventional technologies.

Yttria stabilised zirconia (YSZ) is used as the electrolyte material in commercial solid oxide fuel cells [2]. This is due to its high ionic and low electronic conductivities at the oxygen partial pressures within the cell. However, sufficiently low levels of electronic conductivity and high levels of ionic conductivity are only exhibited at elevated temperatures around 1000°C. Operation at this temperature requires the supporting structure of the active components of the cell to be manufactured from relatively expensive nickel/chromium based alloys, consequently adding significantly to the total manufacturing cost of the fuel cell.

Constructing the cell from cheaper stainless steel components could reduce the total cost; however this would require the operating temperature to be lowered. Operation at reduced temperatures has the additional advantage of reducing sealing problems within the cell. Doped ceria exhibits higher ionic conductivity than zirconia and is a likely candidate as a replacement. Fuel cells with doped ceria electrolytes have been successfully constructed and tested on a laboratory scale [3, 4]. However, due to its electronic conductivity, operation at intermediate temperatures, around 500 to 600°C, is required. Under typical operating conditions cell power loss arising from electronic conductivity in the electrolyte due to reduction at the fuel electrode, would not be detrimental [5, 6].

Desirable mechanical properties are exhibited by partially stabilised zirconia due to transformation toughening. The stress concentration around the tip of a crack induces the tetragonal to monoclinic phase transformation within the crystal lattice. This transformation is associated with a volume increase of approximately 4%, which is sufficient to put the crack tip into compression thus reducing the rate of propagation. Introduction of zirconia into other ceramic materials has been demonstrated to be an effective method for improving mechanical properties.

This paper describes the manufacture of novel composite electrolytes consisting of tetragonal zirconia particles within a gadolinia doped ceria matrix. A number of different particle sizes were produced by calcining over a range of temperatures prior to deagglomeration by grinding or ball milling.

2. Experimental methods

2.1. Sample manufacture

2.1.1. Production of tetragonal zirconia particles

Particles were prepared from 3% yttria stabilised zirconia powder manufactured by Melox. Different sized particles were produced using a two-stage process; the initial stage involved calcining the powder at temperatures between 1100 and 1600°C. Grinding in an agate pestle and mortar or ball milling with zirconia grinding media was used to break the agglomerates formed during the initial calcining stage. Details of the methods used to manufacture each particle type are given in Table I.

TABLE I Method used to manufacture zirconia particles

Sample	Calcining temperature	Deagglomeration procedure
NC	Not calcined	–
11PM	1100	Grind in pestle and mortar by hand
12PM	1200	Grind in pestle and mortar by hand
13PM	1300	Grind in pestle and mortar by hand
14MD	1400	Ball mill dry for 5 hours
15MW	1500	Ball mill in isopropanol for 24 hours
16MD	1600	Ball mill dry for 5 hours

2.1.2. Fabrication of ceramic samples

All the composite samples produced consisted of a $Ce_{0.8}Gd_{0.2}O_{1.9}$ matrix surrounding 5% zirconia particles by weight. Powders were mixed by milling in isopropanol for 1 hour. Only a small amount of zirconia grinding media was added to ensure adequate mixing without the 'tumbling' action of the media reducing the particle sizes unacceptably. Powders were dried under a heat lamp and sieved prior to pressing in a 15 mm diameter cylindrical die at 100 MPa. 1 gram of powder was used in each tablet, which produced a sintered sample of thickness approximately 1.1 mm. Following die pressing the samples were cold isostatically pressed at 150 MPa for ninety seconds before sintering at 1500°C for 4 hours.

2.2. Porosity measurements

Sample porosity, was calculated using a mercury displacement method. This involved measuring the weight of the sintered sample, m, and the force exerted by the sample when completely submerged in mercury (upthrust), u. The sample weight was used to calculate the volume, not including pores, v, from the theoretical density of gadolinia doped ceria and zirconia, ρ_s. Due to the high surface tension of mercury when a porous sample is submerged, the mercury is unable to penetrate the pores. This allows the sample volume, including pores, v_p, to be calculated from the density of mercury, ρ_{Hg}, and upthrust when submerged. Equations, 1–3, were used to calculate percentage porosity.

$$v = \frac{m}{\rho_s} \tag{1}$$

$$v_p = \frac{u}{\rho_{Hg}} \tag{2}$$

$$\%\text{Porosity} = \frac{v_p - v}{v_p} \cdot 100\% \tag{3}$$

2.3. Surface polishing

Due to the different morphologies and sizes of the zirconia particles added to each sample, variations in surface roughness were observed between batches. In order to ensure consistency of results it was necessary to polish all sample surfaces to the same finish. This was particularly important for biaxial flexure strength determination as cracks can initiate from defects on the surface, and essential for fracture toughness as cross sections of samples were used which required surface preparation. Samples were firstly flattened using a range of silicon carbide papers up to a finest grit size of 2500. Scratches were removed using aqueous based 3 μm diamond suspension on a Buehler Texmet-1000 cloth. Subsequent polishing stages were found to cause grain pull out and were therefore omitted.

2.4. Biaxial flexure strength

Biaxial flexure strength (modulus of rupture, MOR) of the ceramic composites was calculated from the force required to fracture a disc in the ball and ring configuration. The ball and ring jig was mounted in an Instron 1122 universal testing machine in conjunction with a load cell (500 kg maximum full range defection). At the beginning of each test the full range deflection was set to as low a level as possible in order to increase the accuracy that loads could be measured from the chart. Applied load and the corresponding cross-head displacement, during each test, were recorded using a chart recorder. The test was carried out in accordance with the standard test method for ceramic substrates [7]. Flexure strength, σ_{max}, was calculated from the failure load, F, Poisson's ratio, v, specimen thickness, t, specimen radius, R, support ring radius, a, and radius of the section under maximum stress, b, using Equation 4. An approximation of $b = t/3$ can be made since t is much greater than the contact radius with the sample surface.

$$\sigma_{max} = \frac{3F(1+v)}{4\pi t^2}\left[\frac{(1-v)(2a^2-b^2)}{(1+v)2R^2} + 2\ln\left(\frac{a}{b}\right) + 1\right] \tag{4}$$

2.5. Fracture toughness

Fracture toughness can be obtained from mechanical tests, however a simpler approach is to use an indentation technique. When a ceramic is indented with a Vickers pyramid indentor radial cracks are generated from the corners of the pyramid indent, where the highest stress concentration occurs, which propagate outwards. Anstis, has shown that the lengths of these cracks, in relation to the dimensions of the pyramid, Fig. 1, are related to the material's fracture toughness, K_{IC}, [8].

In order to obtain a value for fracture toughness it is necessary to obtain the Vickers hardness number for the material, using Equation 5.

$$H_v = 1854.4\frac{P}{d^2} \quad (d = 2a) \tag{5}$$

The Vickers hardness number is then used in Equation 6, in addition to Young's modulus, E(205 GPa [2]),

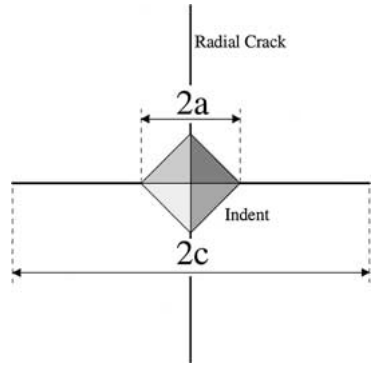

Figure 1 Measurements taken from Vickers indentation.

force, P, and crack length, c, to calculate fracture toughness.

$$K_{IC} = 0.016\left[\frac{E}{H_v}\right]^{1/2}\left[\frac{P}{c^{3/2}}\right] \quad (6)$$

2.6. Scanning electron microscopy

Examination of the samples in an SEM was carried out on fracture surfaces obtained from pieces remaining after biaxial flexure strength measurements and also on polished cross-sections, prepared similarly to samples used for fracture toughness determination. All surfaces were coated in a thin layer of gold, using an Edwards sputter coating unit, to prevent charging. Images were obtained using a Jeol 6310 scanning electron microscope. A beam voltage of 15 kV was used in conjunction with a spot size of 8.

2.7. X-ray diffraction

An analysis of each sample was carried out using x-ray diffractometery. Diffraction patterns were obtained using a Philips PW1730/00 x-ray diffractometer emitting copper k_α radiation of wavelength 1.5405 Å. Scans were produced over a 2-theta range of 25 to 65 degrees. A step size of 0.01° was used with a scanning rate of 0.5 seconds per step.

2.8. Impedance spectroscopy

The electrical properties of the ceramic composites were measured using impedance spectroscopy. A Solatron 1260 gain phase analyser was used to determine the material's impedance over frequencies in the range of 1 Hz to 10 MHz. A DC potential of 0 V and an AC amplitude of 1000 mV were used for all measurements. 20 readings were taken per decade on a logarithmic scale. Solatron software 'Z-plot' was used to construct 'complex plane' plots from the raw data, and to calculate resistance values by circle fitting. From the resistance, R, sample thickness, t, and cross sectional area, A, sample conductivity, σ, was calculated using Equation 7.

$$\sigma = \frac{t}{RA} \quad (7)$$

Impedance data was collected, within the specified frequency range, for each sample between 500 and 700°C at intervals of 50°C. From the sample conductivity, at each temperature, the activation energy for ionic conduction was calculated. The true activation energy for charge migration is included in the process enthalpy in addition to associated energy terms for defect formation [9]. The process enthalpy, ΔH_σ (eV), can be related to conductivity, temperature, T, Boltzmann's constant, k, and a pre-exponential factor, A_σ, using Equation 8.

$$\sigma T = A_\sigma \exp\left[\frac{-\Delta H_\sigma}{kT}\right] \quad (8)$$

If logs to the base e are taken from Equation 8 the relationship between $\ln(\sigma T)$ and $1/T$ is linear. This therefore allows the process enthalpy be obtained from the gradient of data plotted using these values.

3. Results and discussion

3.1. Structural examination

Fracture surfaces and polished cross-sections from the manufactured samples were examined in the SEM to identify any structural differences. Images of the fracture surfaces are shown in Fig. 2a–h. A small amount of finely dispersed closed porosity is visible in all samples. Density measurements suggest that the porosity ranges between 2 and 5%. Areas of increased porosity were identified in all samples, a typical example is shown in Fig. 2h.

Polished sections of each composite sample were examined in the SEM. Again, closed porosity was identified in all images obtained. Fig. 3 shows a typical section from a composite containing uncalcined zirconia particles. Uniform porosity is visible throughout the whole area. A higher magnification image of a different area of the same sample is shown in Fig. 4. An area of higher porosity is visible in the central region. These areas are believed to correspond to where a zirconia particle was present before sintering. However attempts to confirm this by measuring the zirconia concentration using energy dispersive analysis of x-rays (EDAX) were unsuccessful due to the high levels of porosity.

3.2. X-ray diffractometry

X-ray diffraction patterns obtained from sintered samples are shown in Fig. 5. All peaks on the diagram are labelled with the corresponding oxide and crystallographic plane. Normalisation of patterns was achieved by adjusting the cerium oxide (111) peaks to a value of 100. Patterns are staggered along the vertical axis in order to make comparison easier. Similarities in structure between cerium and gadolinium oxide result in the main peaks being superimposed, for this reason planes from both structures are labelled on the diagram. Due to the relatively low concentration of zirconia added (5%), the peaks originating from the (111) and (202) planes are only identifiable on some patterns. They are most pronounced on patterns 13PM and 14DM and 16DM. These correspond to the samples that would be expected to contain the largest TZP particles.

3.3. Biaxial fracture strengths

Average biaxial flexure strengths are given in Fig. 6 where error bars represent one standard deviation. Data for a gadolinia-doped ceria sample containing no zirconia particles is also plotted for comparison. Samples 11PM, 12PM and 13PM were calcined at 1100, 1200 and 1300°C respectively prior to deagglomeration using a pestle and mortar. The main effect of calcining is to densify and partially sinter particles, therefore it follows that as calcining temperature is increased the ease at which the agglomerated particles can be broken reduces. The decrease in composite strength is a direct consequence of the increasing size of the agglomerated zirconia particles.

Agglomerates of zirconia calcined at 1400, 1500 and 1600°C were found to be to hard to break by hand using a pestle and mortar. For this reason a ball mill was used. Samples 14DM and 16DM, which contained zirconia particles calcined at 1400 and 1600°C respectively,

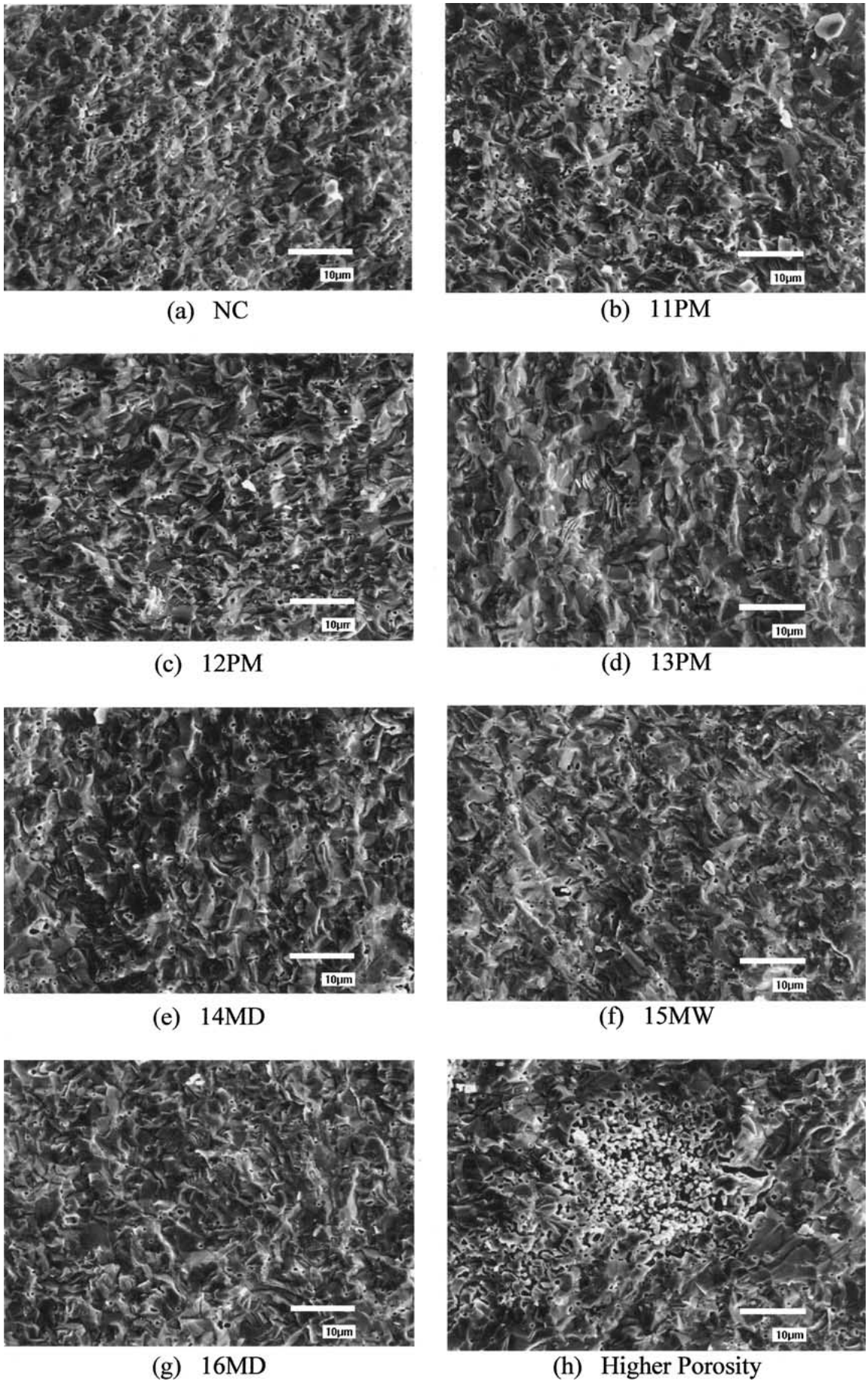

Figure 2 (a–h) Fracture surfaces of composite samples (For sample codes, see Table I).

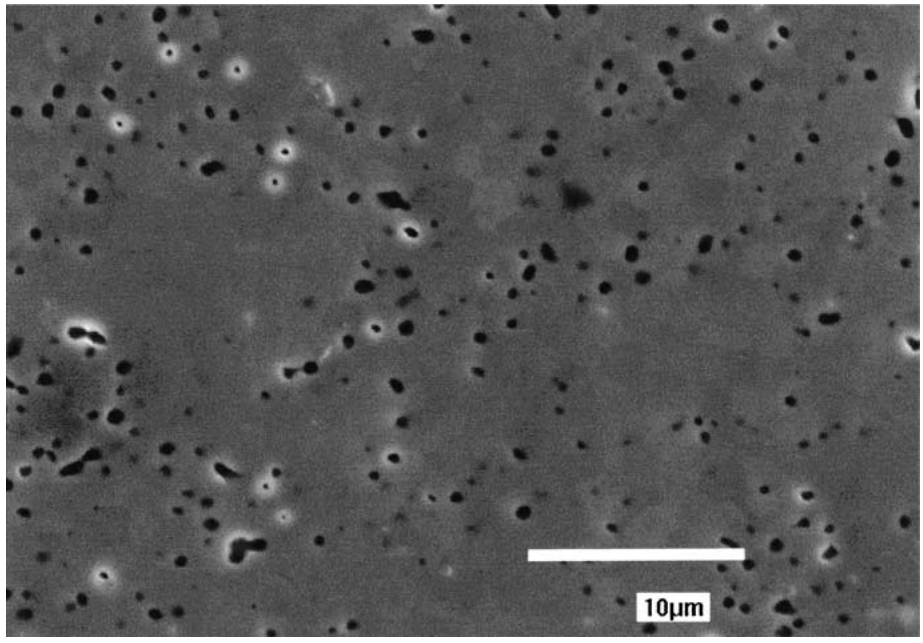

Figure 3 Polished cross-section of sample containing uncalcined zirconia particles.

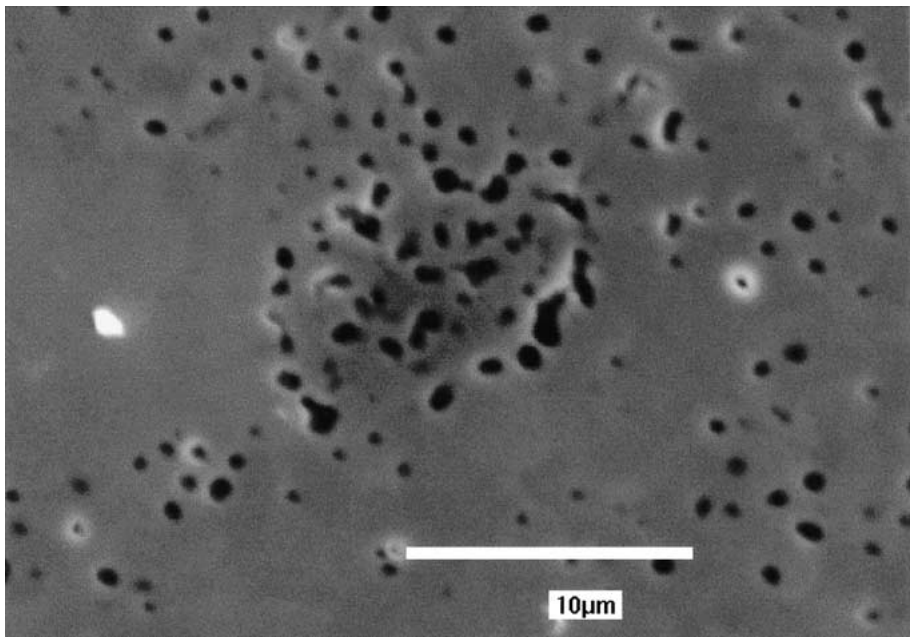

Figure 4 High magnification image of a polished cross-section from a sample containing uncalcined zirconia particles showing an area with increased porosity.

were ball milled dry for 5 hours. Both the composites produced using these particles have approximately the same fracture strength, however it is interesting to note that the standard deviation of sample 16DM is the smallest. Zirconia particles calcined at 1500°C were wet milled in isopropanol for 24 hours, sample 15WM. Wet milling is more efficient than dry milling and significantly reduced the particle size. This is reflected by the increase in fracture strength compared to pure gadolinia doped ceria and sample UC, which contained the uncalcined zirconia particles and pure gadolinia doped ceria.

3.4. Fracture toughness

A value for the fracture toughness of each composite sample was obtained using an indentation method. Fracture toughness ranged between 0.76 and 1.02 MPa $m^{-1/2}$, values were all within experimental error, suggesting that there is no significant difference in fracture toughness between samples. It should be noted that for a number of samples the TZP particle size and indent area are comparable in size. This suggests that in some instances particle size may influence the fracture toughness values obtained independently of macroscopic properties.

3.5. Electrical properties

Data obtained by complex impedance analysis is presented in the form of complex plane plots, real impedance Z' versus imaginary impedance Z''. Complex plane plots containing data over the range of temperatures corresponding to each composite sample is shown in Fig. 7.

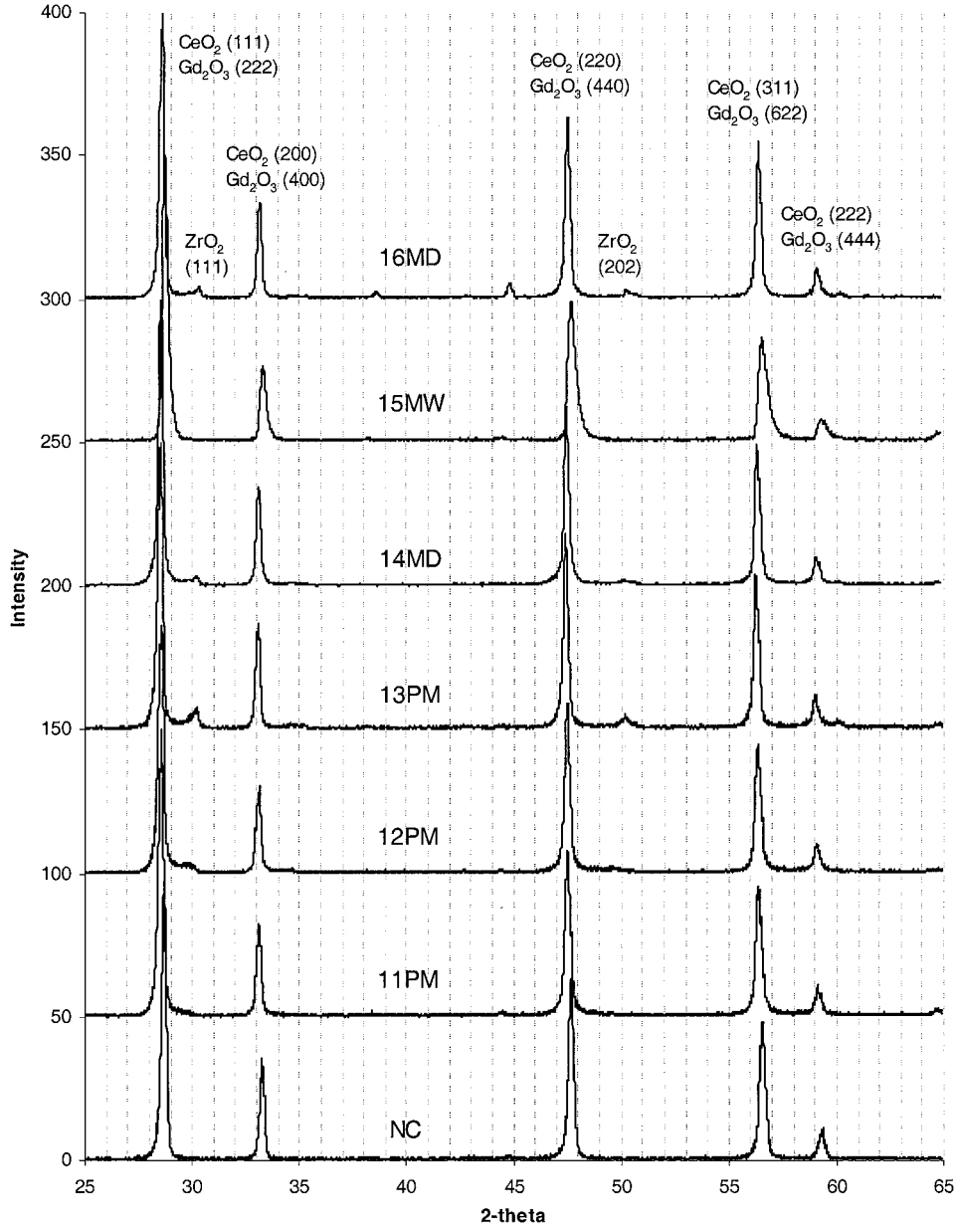

Figure 5 X-ray diffraction patterns for composite samples tested (For sample codes, see Table I).

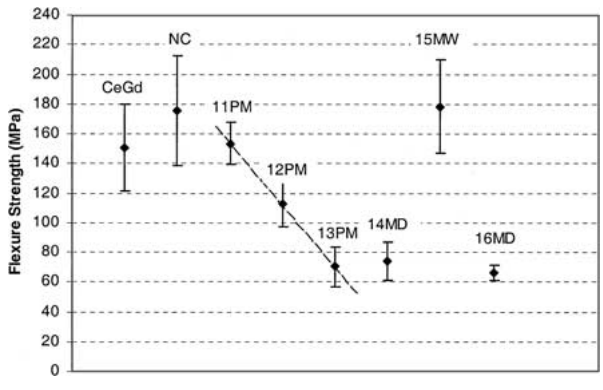

Figure 6 Biaxial flexure strengths (Modulus of Rupture) of composite samples (For sample codes, see Table I).

All the data follows the same trend, which consists of a semicircle starting at the origin followed by a sloping line. A typical diagram is shown in Fig. 7h. This differs somewhat from the idealised complex impedance plot shown in Fig. 8. Semicircles observed in the plots are associated with the grain interior resistance, as additional semicircles, which would normally be associated with the grain boundary, are not visible.

This result is consistent with observations made by Christie and Van Berkel on 20% gadolinia doped ceria [10]. Two semicircles were identified on plots from samples sintered at 1400°C or below, and one semicircle on samples sintered above this temperature. Micro structural studies indicated that the increased grain size associated with higher sintering temperatures was the cause.

Plots of log conductivity multiplied by temperature, $(\ln(\sigma T))$, versus the inverse of temperature are shown in Fig. 9 for each sample. The correlations, R^2, of the trend lines shown in the figure, are all in the range 0.9870–0.9997 indicating a good fit to the data. Calculated values of the activation energies, obtained from the slopes of the lines, are shown in Fig. 10. These are all in the range 0.79 to 1.05 eV and within the experimental error and hence any differences cannot be considered significant.

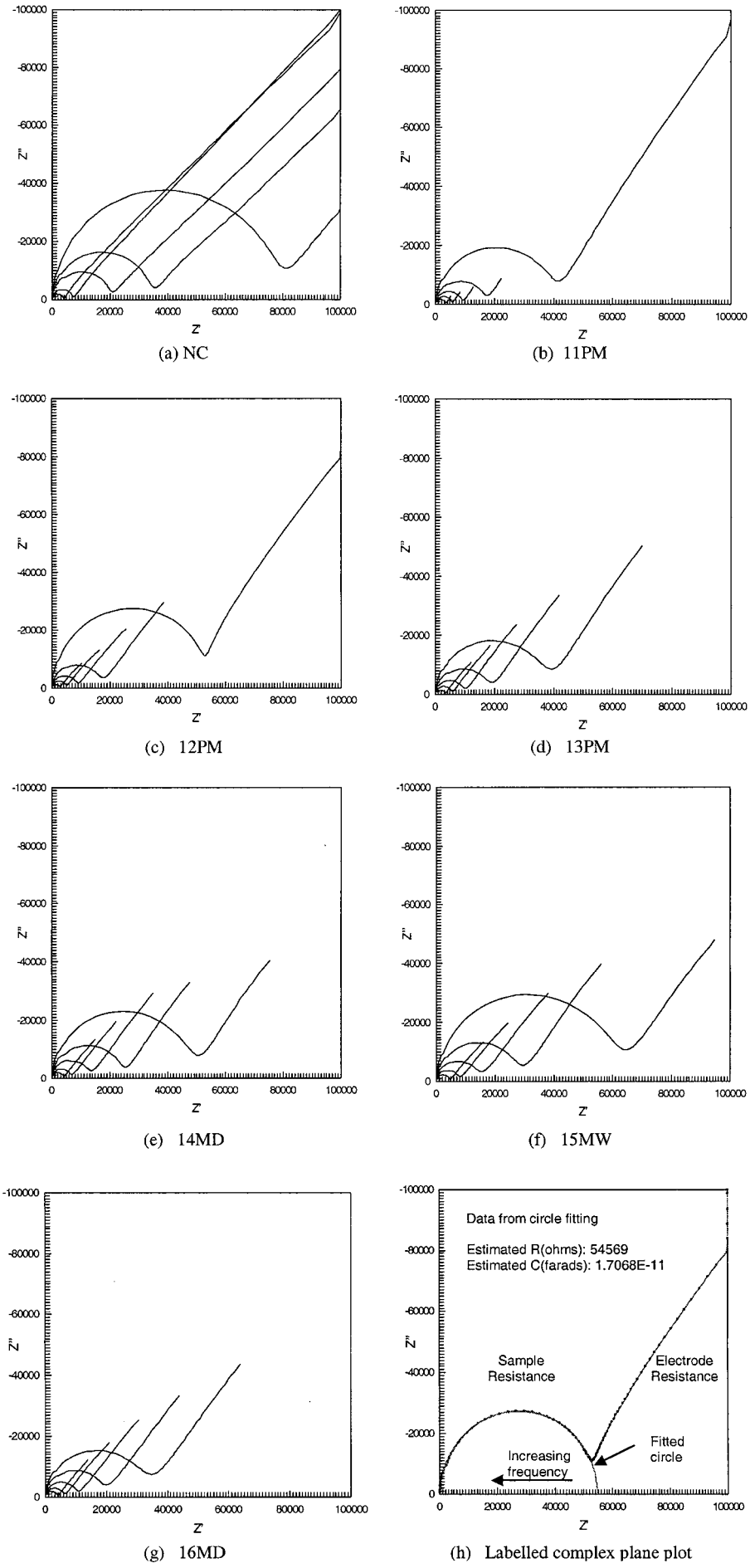

Figure 7 (a–h) Complex plane plots of composite samples between 500 and 700°C (For sample codes, see Table I).

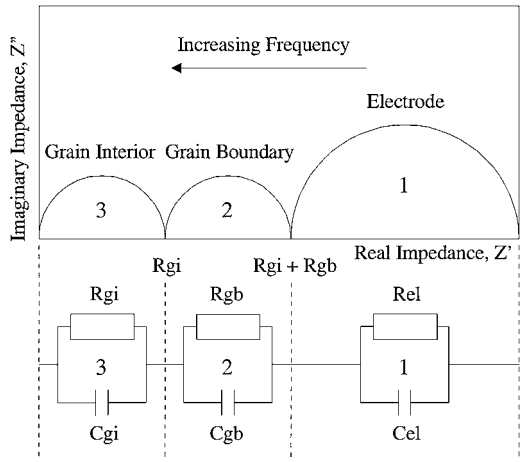

Figure 8 Idealised complex plane plot and equivalent circuit for a ceramic material.

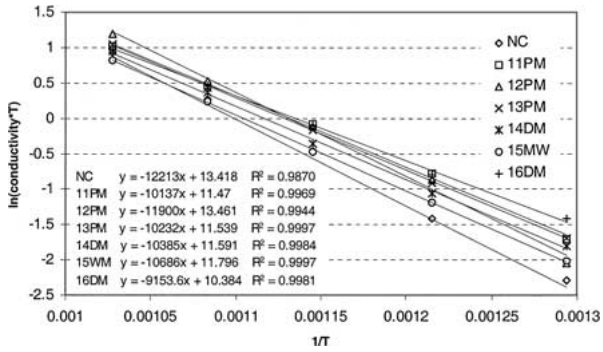

Figure 9 Plot of ln(conductivity*temp) versus $1/T$ (For sample codes, see Table I).

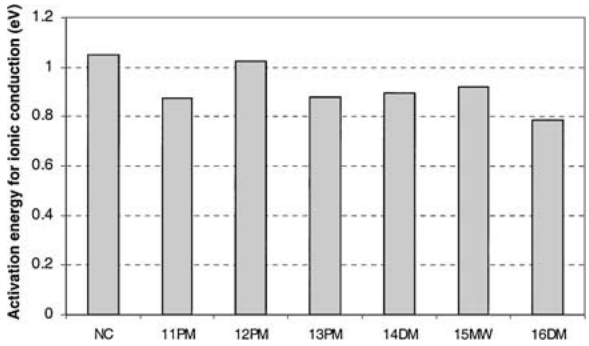

Figure 10 Activation energies for ionic conduction for composite samples (For sample codes, see Table I).

4. Conclusions

1. Addition of zirconia particles can increase the flexure strength of gadolinia doped ceria ceramics.

2. Large agglomerate particles can act as an area of stress concentration leading to a reduced flexure strength.

3. Zirconia particles are the likely cause of areas of higher porosity within the ceramic.

4. Fracture toughness of the composite does not change significantly with the type of particle added. However, is should be noted that this may be a consequence of the indentation method used to obtain values.

5. Only one semicircle was observed on the complex plane plots. This is believed to be due to an increased grain size associated with the sintering temperature of 1500°C.

References

1. S. P. S. BADWAL and K. FOGER, *Ceramics International* **22** (1996) p. 257.
2. J. E. SHEMILT, H. M. WILLIAMS, M. J. EDIRISINGHE, J. R. G. EVANS and B. RALPH, *Scripta Met & Mat*, in press.
3. N. Q. MINH, *Journal of the American Society* **76** (1993) p. 563.
4. E. EGUCHI, T. SETOGUCHI, T. INOUE and H. ARAI, *Solid State Ionics* **52** (1992) p. 165.
5. B. C. H. STEELE, "Ceramic Oxygen Ion Conductors and Their Technological Applications," edited by B. C. H. Steele (Institute of Materials, London, 1996) p. 151.
6. D. SCHNEIDER, D. GÖDICKEMEIER and L. J. GAUKLER, "Ceramic Oxygen Ion Conductors and Their Technological Applications," edited by B. C. H. Steele (Institute of Materials, London, 1996) p. 103.
7. Standard test method for Biaxial Flexure Strength (Modulus of Rupture) of Ceramic Substratesm, ASTM Designation: F 394-78 (Reapproved 1991).
8. G. R. ANSTIS, P. CHANTIKUL, B. R. LAWN and D. B. MARSHALL, *Journal of the American Ceramic Society* **64**(9) (1981) p. 533.
9. J. A. KILNER and R. J. BROOK, *Solid State Ionics* **6** (1982) p. 237.
10. G. M. CHRISTIE and F. P. F. VAN BERKEL, *ibid.* **83** (1996) p. 17.

Received 9 November 2001
and accepted 22 May 2002